Geophysical Research Letters

RESEARCH LETTER
10.1029/2023GL105660

Special Collection:
Recent Discoveries in Substorm Research

Evolution of Energetic Proton Parallel Pressure Anisotropy at Geosynchronous Altitudes: Potential Role in Triggering Substorm Expansion Phase Onset

S. S. Babu[1], I. R. Mann[1], S. Dimitrakoudis[1], L. G. Ozeke[1], I. J. Rae[2], C. Forsyth[3], and A. W. Smith[2]

[1]Department of Physics, University of Alberta, Edmonton, AB, Canada, [2]Department of Mathematics, Physics and Electrical Engineering, Northumbria University, Newcastle, UK, [3]Mullard Space Science Laboratory, University College London, Dorking, UK

Abstract The sequence of events associated with the triggering of energy release during substorm expansion phase onset is still not well-understood. Oberhagemann and Mann (2020b, https://doi.org/10.1029/2019gl085271) proposed a new substorm onset mechanism, where the transition toward parallel proton pressure anisotropy during tail stretching in the late growth phase could trigger a pressure anisotropic ballooning instability. Here we examine the evolution of energetic proton parallel pressure anisotropy at geosynchronous altitudes, seeking evidence in support of the proposed substorm onset mechanism. We use the Geostationary Operational Environment Satellite (GOES) proton flux and magnetometer data combined with substorm onset indicators derived from ground-based magnetometers. Superposed epoch analysis of substorm onset times for 2014 using the isolated substorm list (Ohtani & Gjerloev, 2020, https://doi.org/10.1029/2020ja027902) clearly shows signatures of energetic proton parallel pressure anisotropy immediately before substorm onset, potentially supportive of the Oberhagemann and Mann theory.

Plain Language Summary Substorms are disturbances in the nightside region of the geospace associated with the rapid release of stored magnetic energy. In the ionosphere, the signatures of this energy release are the spectacular dancing lights known as aurorae (northern and southern lights). The processes that lead to energy storage are well-known. However, there are competing theories on what triggers the release of this significant amount of energy at substorm onset. According to a new substorm onset theory proposed by Oberhagemann and Mann, when the magnetic field stretches in the nightside during the energy storage, the pressure becomes more parallel to the magnetic field, leading to a ballooning instability at substorm onset. Here, we look for observational support for the association of such pressure profile at geosynchronous altitudes with substorm onset to examine the proposed model. Superposed epoch analysis of isolated substorms in 2014 shows increasing energetic proton parallel pressure anisotropy at the onset, providing evidence to support the Oberhagemann and Mann theory.

Key Points:

- Oberhagemann and Mann theory proposes that proton parallel temperature anisotropy triggers ballooning instability leading to substorm onset
- We use pitch angle resolved energetic proton fluxes at geosynchronous altitudes seeking observational evidence in support of the model
- Superposed epoch analysis of isolated substorms shows signatures of increasing energetic proton parallel anisotropy which peaks near onset

Supporting Information:

Supporting Information may be found in the online version of this article.

Correspondence to:

S. S. Babu,
sbabu@ualberta.ca

Citation:

Babu, S. S., Mann, I. R., Dimitrakoudis, S., Ozeke, L. G., Rae, I. J., Forsyth, C., & Smith, A. W. (2024). Evolution of energetic proton parallel pressure anisotropy at geosynchronous altitudes: Potential role in triggering substorm expansion phase onset. *Geophysical Research Letters*, *51*, e2023GL105660. https://doi.org/10.1029/2023GL105660

Received 19 JAN 2024
Accepted 2 MAY 2024

1. Introduction

Geomagnetic substorms are disturbances in the Earth's magnetosphere triggered by the release of stored energy in the magnetotail (Akasofu, 1964; McPherron, 1979). Although the major phenomena that occur during the auroral substorm are well-established (e.g., Akasofu, 2017; Henderson, 2021, and references therein), the corresponding sequence of events in the magnetosphere remains hotly debated (e.g., Angelopoulos et al., 2008; Lui, 2003; Lui et al., 2008; Ohtani, 2001). The substorm has three phases: growth, expansion, and recovery. The expansion phase ultimately results in the release of stored magnetic energy in the magnetotail, the injection of energetic particles toward the Earth (e.g., McPherron, 1979; McPherron et al., 1973) and a dipolarization of the tail magnetic field (e.g., McPherron et al., 1973). Correspondingly, the expansion phase in the ionosphere is associated with a brightening and poleward and westward expansion of the aurora (Akasofu, 1965; McPherron, 1979), and the onset is usually marked by the sudden brightening of the most equatorward arc (Akasofu, 1977), and the structuring of the onset arc in the form of auroral beads (e.g., Kalmoni et al., 2017, and others).

There are opposing views on the physical processes that occur in the magnetosphere at the beginning of the expansion phase, which typically falls under two overarching concepts: the near-Earth neutral line (NENL) model, where the onset occurs due to reconnection of magnetic field lines at distances between around 10 to 20 R_E

(Baker et al., 1996), and the current disruption (CD) model, where the onset occurs due to a disruption of the cross-tail current that could be triggered by a variety of possible plasma instabilities in the near-Earth plasma sheet (Lui, 1991; Lui et al., 1991; Rae et al., 2009) (see also Lui, 2004, and references therein, for a review). In the latter model, instabilities such as cross-tail current instability or ballooning instability could trigger the onset (Lui, 1991; Lui et al., 1991). These two paradigms are also often described in terms of the direction of propagation of the sequence of events, being characterized as outside-to-in and inside-to-out, respectively (e.g., Sergeev et al., 2012, and references therein). Rae et al. (2010) compared the spatial and temporal evolution of beads and structuring along the onset arc to a range of possible plasma sheet instabilities (cf. Lui, 2004), which have been postulated to be associated with onset, under the assumption that the equatorial structures map into the ionosphere as a result of coupling to kinetic Alfvén waves (Kalmoni et al., 2018; Smith et al., 2020).

A recent study by Oberhagemann and Mann (2020b) proposed a new substorm onset mechanism, which specifically suggested a role for pressure anisotropic ballooning instability triggered by the transition toward parallel pressure anisotropy as a result of tail stretching during the growth phase. Furthermore, they discussed how the parallel temperature anisotropy could be formed naturally due to the competition between betatron and Fermi acceleration as the tail stretched. See also the modeling of particle trajectories completed by Oberhagemann and Mann (2020a), which further supported this hypothesis. Observational evidence for the association of increasingly parallel pressure with substorm onset would provide the first step toward testing the Oberhagemann and Mann onset theory, which can be addressed by analyzing satellite data sets with the required pitch angle distributions (PADs). Geosynchronous orbits are considered as they sample regions close to the inner edge of the plasma sheet (Denton, 2005) and the transition from dipole-like to tail-like field lines. Parameters such as the pressure gradient and plasma beta, which are destabilizing, should be locally high at the inner edge of the plasma sheet (see e.g., Oberhagemann & Mann, 2020a, 2020b, for further discussion). As the growth phase continues, these parameters increase during the growth phase tail stretching until the ballooning instability threshold is exceeded, after which substorm onset occurs (Oberhagemann & Mann, 2020b). The key point from the Oberhagemann and Mann (2020b) model is that the parallel temperature anisotropy, which develops during the late growth phase, should lower the instability threshold, resulting in a transition from marginal stability to onset.

In the following, we use the Legendre fitting technique as discussed in Y. Chen et al. (2014), to show that the proton PADs at geosynchronous altitudes become increasingly parallel anisotropic toward substorm onset, consistent with the Oberhagemann and Mann (2020b) theory.

2. Data and Methods

We use superposed epoch analysis for a duration of ±6 hr from the onset of isolated substorms in the calendar year 2014 to examine energetic proton signatures and their related PADs observed at geosynchronous orbit. The isolated substorm list from Ohtani and Gjerloev (2020) is used, which identifies the onsets of isolated substorms (~865 substorms in 2014) using the SuperMAG SML index (Newell & Gjerloev, 2011) in a three-step process, and provides substorm onset times and the location of the closest magnetometer station to onset on the ground. Data from the MAGnetospheric Proton Detector (MAGPD) and Magnetometer (MAG) instruments on the National Oceanic and Atmospheric Administration (NOAA) Geostationary Operational Environment Satellite (GOES) 13 and GOES 15 satellites provide pitch-angle resolved magnetospheric energetic proton flux and magnetic field data, respectively. The satellites provide good coverage with northern magnetic conjugate footpoints over Canada, where relatively dense two-dimensional magnetometer station coverage from arrays contributing to the SuperMAG consortium (Gjerloev, 2012), including from the Canadian Array for Realtime InvestigationS of Magnetic Activity (CARISMA) (Mann et al., 2008), further allow the location and timing of the ground onsets to be understood relative to the location of the GOES satellites in space.

The in situ data is analyzed by dividing it into different sectors based on the relative geographic longitude of the satellite magnetic footprint as compared to the ground onset location. We select a 30° longitude window to both the east and west of each of these satellites to assess the PADs around the time of the ground onset. Note that this means the spacecraft local time could be within the range of ±2 hr from the ground onset location. To specifically study onsets in the near-midnight local time sector, we further only select ground onsets in the range between 21 and 3 MLT. There are 301 and 156 isolated substorms in GOES 15 and GOES 13 sectors, respectively. The supplementary material contains a summary of the properties of the events in each sector and the superposed epoch analysis of the magnetic field observed by both GOES satellites in the spacecraft Earth Polar (Parallel)

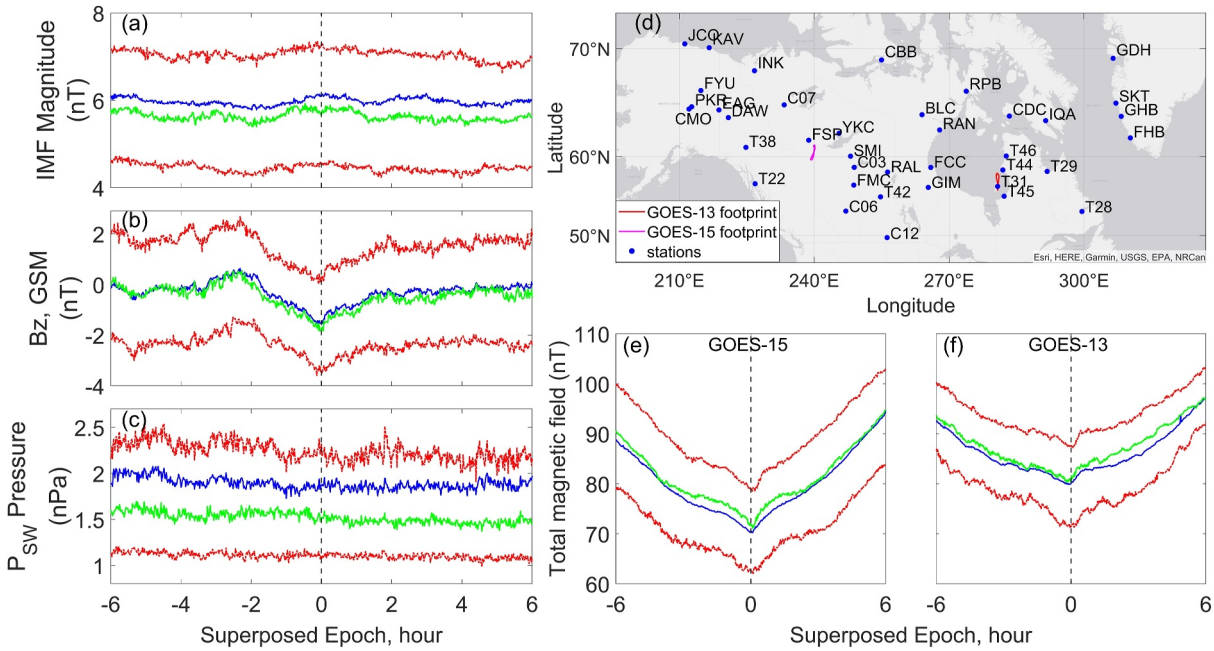

Figure 1. Superposed epoch of (a) Average interplanetary magnetic field (IMF) magnitude (b) z component of the IMF in geocentric solar magnetospheric (GSM) coordinates, and (c) solar wind dynamic pressure for isolated substorm events in 2014 (Ohtani & Gjerloev, 2020). (d) Ground magnetometer stations coverage in the 195°E to 315°E longitude range, and northern magnetic footprints of the GOES-15 and GOES-13 satellites, on 5 January 2014. Panels (e) and (f) show superposed epoch analysis of the average total magnetic field for both GOES-15 and GOES-13 for the 2014 substorm onsets from panels (a)–(c). In each panel, the blue line is the mean; the green is the median, and the two red lines represent the lower and upper quartiles in the superposed distributions.

Normal (EPN) coordinate system, where P is directed northward and normal to the orbital plane, E is Earthwards, and N points Eastward completing the triad in the E cross P direction (e.g., Loto'aniu et al., 2020).

Figures 1a–1c shows a summary of the superposed epoch analysis of the magnitude of the interplanetary magnetic field (IMF), the geocentric solar magnetospheric (GSM) z-component of the IMF, and the solar wind dynamic pressure for the isolated substorm onsets in 2014 which are used in this study. In each panel, the mean, median, and lower and upper quartiles are shown in blue, green, and red, respectively. We used the modified high-resolution 1-min average OMNI data (King & Papitashvili, 2005). Interestingly, Figure 1b shows strong evidence of a northward turning IMF in the ensemble of substorm onsets, with the superposed mean, median, and lower and upper quartiles all showing the same trend toward more positive (less negative) GSM B_z at epoch zero. As previously discussed by Morley and Freeman (2007) and Freeman and Morley (2009), even though we observe a northward turning of the superposed IMF at the time of substorm onset, this does not necessarily imply that such northward turnings can be identified as a causal explanation for the triggering of individual substorm onsets.

Figure 1d shows the available ground magnetometer stations in the longitude range defined above, as well as the location of the magnetic field line trace to the northern hemisphere for GOES 13 and 15 on 5 January 2014, at 04:17 UT, calculated using the T89 magnetic field model (Tsyganenko, 1989). A detailed list of station names and their geographic locations is provided in the Appendix. Figures 1e and 1f show the results from a superposed epoch analysis of the magnetic field magnitude measured by the outboard magnetometer (Rodriguez, 2014) from both GOES 15 and 13 satellites, respectively, using the same line colors for the mean, median and the quartiles as in panels (a)–(c). A decrease in magnetic field magnitude during the growth phase, and an increase during the expansion phase, separated by a sharp discontinuity at the onset time at zero epoch, is apparent in the data from both satellites. This appears to be a characteristic across the ensemble of the changes in the magnetic field at geosynchronous orbits at onset, clearly defined in both quartiles, the mean and median of the magnetic field magnitudes, as expected in in situ monitoring.

To characterize the evolution of the proton PADs at GOES, we use the proton flux data from the MAGPD instrument on the Space Environment Monitor (SEM) subsystem. MAGPD has nine detector telescopes oriented in

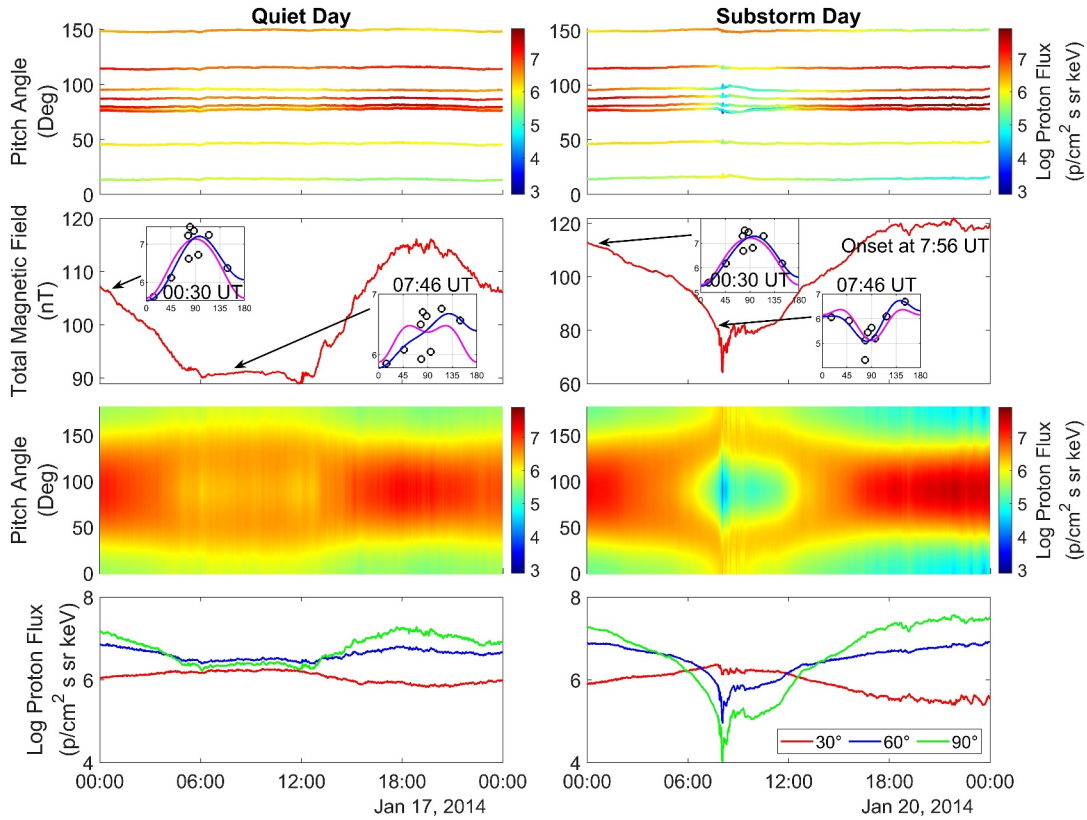

Figure 2. Quiet day and substorm day analysis on 17 January 2014 (left column) and 20 January 2014 (right column), respectively, using Geostationary Operational Environment Satellite (GOES) 15 satellite data. Rows from top to bottom for each day: Logarithm of 140 keV proton flux as a function of pitch angle for the nine MAGnetospheric Proton Detector (MAGPD) telescopes; total magnetic field measured by GOES 15 magnetometer; Logarithm of proton flux as a function of pitch angle using Legendre polynomial fitting; Proton fluxes at fixed pitch angles of 90° (green), 60° (blue), and 30° (red) derived from the Legendre polynomial fits. Insets in the second row show examples of Legendre polynomial fitting of the logarithm of proton flux (*y*-axis) to create continuous pitch angle distributions (PADs) from the nine telescopes to pitch angle (*x*-axis) ranging from 0° to 180° for two different times; symbols are the nine data points from MAGPD, the blue line shows the fitting using all (even and odd) Legendre coefficients and the magenta line for fitting using only even Legendre coefficients.

35° increments, where the central telescope faces the zenith direction, two telescopes at each of ±35° and ±70° from zenith, in both the X-Y and Y-Z planes. The instrument measures proton fluxes for energy levels ranging from 80 to 800 keV, including different energy channels at 95, 140, 210, 300, and 575 keV (Jaynes et al., 2013; Rodriguez, 2014; Rowland & Weigel, 2012).

The proton flux data are interpolated to provide a continuous PAD from 0° to 180° using the Legendre polynomial fitting method discussed in Y. Chen et al. (2014) of order 4. Example results from the Legendre polynomial fitting are shown in the inset plots in the second panel of Figures 2 and 3. Note that telescopes 3 and 5 on GOES 15 often show different flux values from those derived from other telescopes in the same pitch angle range, and this is likely due to differential detector degradation over time (B. Kress, personal communication, February 5, 2021). Such data inconsistencies across multiple telescopes are much less apparent in the data from GOES 13. Nonetheless, the multiple look-direction MAGPD data set from both GOES 15 and 13 provides a good basis for assessing the proton PAD evolution through the course of the substorm sequence, especially across substorm onset, from two geosynchronous satellites. This is seen clearly in the example PADs shown in Figures 2 and 3.

For the remainder of the paper, we restrict statistical analysis of the PADs under the approximation of assumed symmetry about 90° pitch angle by using Equation 1 in Y. Chen et al. (2014) and using only even Legendre polynomial coefficients through the course of each isolated substorm. We used the logarithm of fluxes for fitting to avoid negative flux values in the fitted PAD profiles. We include both GOES 15 and 13 data in the analysis to

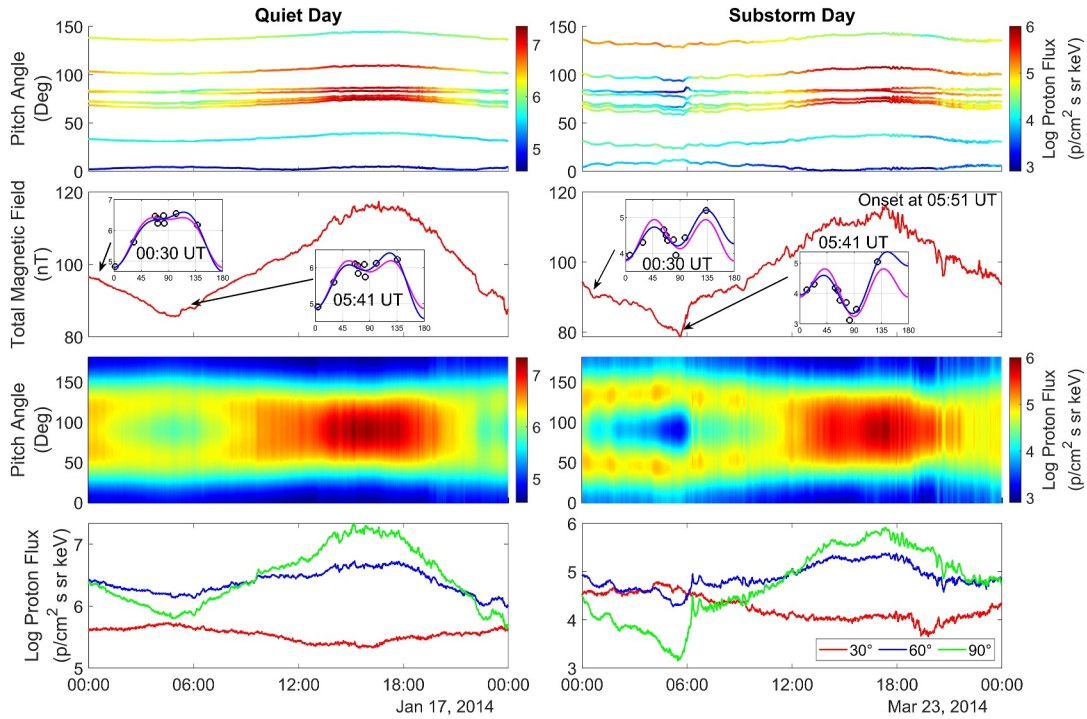

Figure 3. Analysis of example quiet day and substorm day for 17 January 2014 and 23 March 2014, respectively, using GOES-13 satellite data. Same format as Figure 2, and again using 140 keV proton flux.

incorporate a larger number of substorm onsets, noting that the GOES 15 satellite provides coverage closer to the magnetic equator (magnetic latitude ∼4°) than GOES 13 (magnetic latitude ∼10°).

3. Results

We present an example of the Legendre polynomial fitted proton PAD on example quiet (left) and substorm (right) days in Figures 2 and 3, respectively. The example quiet day has no substorm onsets before 12 UT in the isolated substorm list. The panels in the first row show the 140 keV energy channel from the GOES 15 and 13 satellites, respectively, at nine different pitch angles. The panels in the second row show the total magnetic field measured by the outboard magnetometer on the GOES satellites. For GOES 15 data in Figure 2, the substorm onset on 20 January 2014 was at 07:56 UT (identified as being closest to station C07 on the ground in the isolated substorm list). For GOES 13 in Figure 3, on 23 March 2014, the onset was at 05:51 UT (identified as being closest to the ground station T31 in the isolated substorm list). The inset plots show the results from the Legendre polynomial fitting procedure for a single timestep for log proton flux as a function of pitch angle. The examples of the two fits which are presented in the insets in the second row of Figures 2 and 3 are firstly at 00:30 UT, typical of pre-growth phase conditions, and secondly, from a time 10 min before the substorm onset on each day typical of the conditions immediately pre-onset. Note that for the quiet day (left), a fit for the same UT time is shown in the left column to demonstrate the difference in the pre-onset PADs on a quiet day as compared to a substorm day (right). We have included the SuperMAG *SMU* and *SML* indices (Newell & Gjerloev, 2011) for the quiet and substorm days in the Supporting Information S1.

The third panel in Figures 2 and 3 shows the continuous PAD created using the Legendre fitting method with even coefficients for pitch angles ranging from 0° to 180° for a single day. On a quiet day, we observe a typical PAD where the flux peaks at 90° pitch angle during the daytime, and butterfly distribution with flux peaking at around 60° during the nighttime (Sibeck et al., 1987). However, for the substorm day, the higher flux is observed at pitch angles around ∼30°–40°. The fourth panel shows the fluxes at fixed pitch angles of 30°, 60°, and 90°, which are derived from the continuous PADs created by the fit to the Legendre polynomials. It clearly shows that on a quiet day, we observe the typical diurnal development of butterfly PAD as a result of drift-shell splitting (Sibeck et al., 1987). In contrast, on a substorm day, the 90° flux magnitude starts to decrease around 2–3 hr before the

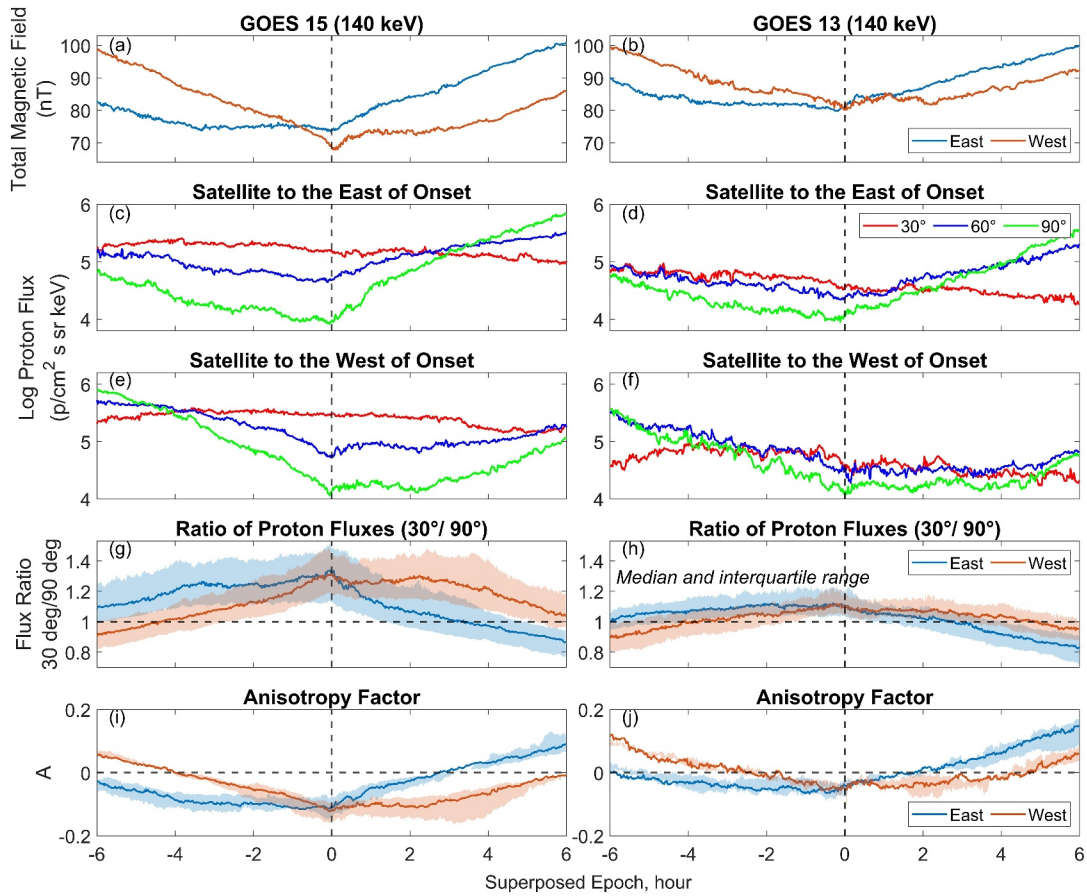

Figure 4. Superposed-epoch analysis of proton fluxes using Geostationary Operational Environment Satellite (GOES) 15 (left) and GOES 13 (right) satellite data, where the ground-based onset time defines epoch zero. Rows from top to bottom for each satellite: Median total magnetic field for the satellite to the east and west of the onset; Median log proton flux when the satellite was to the east of onset; the same when the satellite was to the west of onset; Median and interquartile ratio of 30°/90° proton flux for the satellite to the east and west of onset; Median and interquartile anisotropy factor for the satellite to the east and west of onset. In panels (c)–(f), proton fluxes at fixed 90° (green), 60° (blue), and 30° (red) pitch angles derived from Legendre polynomial fits are shown. Panels (a) and (b) show the total magnetic field, panels (g) and (h) show the ratio of proton fluxes at 30°/90° pitch angles, and panels (i) and (h) show the anisotropy factor calculated using Equation 1, where the respective GOES satellite is to the east (blue) and west (red) of the ground station recording the ground onset in the Ohtani and Gjerloev (2020) substorm list.

onset and is a minimum at the time of onset. Significantly, Figures 2 and 3 show that on a substorm day, the PAD develops to demonstrate clear butterfly distributions with off-equatorial peaks immediately prior to substorm onset. During the late growth phase, the PADs show fluxes with peaks close to 30° and 150° pitch angles and have an increased flux at these pitch angles immediately preceding substorm onset.

To illustrate this behavior in the ensemble of substorm onsets derived from isolated substorms from 2014, Figure 4 shows results from a superposed epoch analysis of isolated substorm onsets for both GOES 15 and 13 satellites using 140 keV proton flux. Here the Ohtani and Gjerloev (2020) onset time defines epoch zero. During the growth phase, about 2–3 hr before the zero epoch, we observe a decrease in the 90° and 60° pitch angle flux with the PADs showing butterfly distributions with their peaks close to 30° and exhibiting the same pattern of minimum flux at 90° and maximum at 30°, as seen for the individual example substorm days. Figures 4g and 4h show the median and interquartile range of ratio of the 30°/90° pitch angle flux for both the satellites, which demonstrates more clearly the increase in the 30°/90° ratio at the zero epoch, the beginning of the expansion phase.

The pressure anisotropy factor, A, for each energy range can be calculated using the following equation (M. W. Chen et al., 1998; De Michelis et al., 1997, 1999):

$$A = \frac{P_{\perp}}{P_{\parallel}} - 1 = \frac{\int J(\epsilon,\alpha)\sin^3\alpha d\alpha}{2\int J(\epsilon,\alpha)\cos^2\alpha \sin\alpha d\alpha} - 1 \quad (1)$$

Here, $J(\epsilon, \alpha)$ represents the flux at energy ϵ and equatorial pitch angle α. The anisotropy factor is computed using Legendre Polynomial fitted flux as a function of pitch angle at GOES 13 and GOES 15. We use in situ rather than equatorial pitch angles due to uncertainties in magnetic field model mapping during the substorm late growth phase. Note also that the 90°, 60°, and 30° pitch angles at GOES 13 and 15 satellites correspond approximately to equatorial pitch angles of (70°, 55°, 28°) and (82°, 59°, 30°), respectively, for a dipolar magnetic field. The strength of the in situ parallel anisotropy seen at GOES 13 is less than that seen at GOES 15 in Figure 4, as a result of the more off-equatorial magnetic latitude of GOES 13. Here, A is an asymmetric factor because A = 1 when $P_{\perp} = 2P_{\parallel}$ and $A = -0.5$ when $P_{\parallel} = 2P_{\perp}$. The median and upper and lower quartiles of A are shown in Figures 4i–4j. Similar features in the distributions of A as a function of substorm onset epoch time are observed across all energy channels ranging from 95 to 300 keV for both GOES 13 and GOES 15 satellites (see Figures S5–S7 in Supporting Information S1). The superposed epoch analysis for both satellites using other energy channels are also included in the Supporting Information S1. Note that at times after epoch time zero the superposed epoch statistics could be influenced by particle injections, depending on the relative locations of the spacecraft and the ground onset.

4. Discussion and Conclusions

The focus of this paper is to seek observational evidence for increasing energetic proton parallel pressure anisotropy during the late growth phase of a substorm, which according to the Oberhagemann and Mann (2020b) theory, might be associated with the triggering of substorms. Very significantly, the ratio of the 30°/90° flux is seen in the superposed epoch analysis statistics to increase at the time of substorm onset. There are a small number of previous works which have reported similar behavior. In terms of electron distributions, Baker et al. (1978) observed that electrons in the energy range of 30–300 keV at geosynchronous altitudes showed variations in the PADs before and after substorm onset, where cigar distributions, with flux peaking in the direction of the magnetic field, are observed prior to substorm onset, that is, during the late growth phase. However, they did not consider the ion distributions. In a superposed epoch analysis of thermal ions and electrons at geosynchronous orbit using the data from the Los Alamos National Laboratory (LANL) Magnetospheric Particle Analyzer (MPA) instrument, Birn et al. (1997) showed that parallel temperature anisotropy dominates during the late substorm growth phase, with signatures weaker in thermal ions and more enhanced in thermal electrons. It is important to note that even though the total ion pressure is influenced by energetic ions, as measured by the LANL higher energy Synchronous Orbit Particle Analyzer (SOPA) instrument, these energetic ions were excluded from the temperature anisotropy calculations in Birn et al. (1997) as the SOPA data was not routinely available. However, the proton energies that are monitored by the GOES MAGPD instrument are in the range that contributes very significantly to the proton pressure at geosynchronous altitudes. For example, Fu et al. (2023) showed in their Figure 4c that the majority of the proton pressure is carried by particles in the 30–300 keV range at $L \sim 6$. Approximately 75% of the pressure is attributed to protons with energies exceeding 30 keV.

Particles with different pitch angles can follow different drift paths even though they start at the same point, commonly termed drift-shell splitting. Lower equatorial pitch angle particles follow more circular drift paths to conserve the second adiabatic invariant, and higher pitch angle particles follow contours of constant magnetic field strength to conserve the first adiabatic invariant (Sibeck et al., 1987). The substorm growth time of a few hours to transition from a less stretched to a more stretched tail maps to the drift time of energetic protons with energies ~30–100 keV. Conservation of the first and second adiabatic invariants can therefore create parallel temperature anisotropy for particles with these energies in the stretching growth phase near-Earth transition region magnetic field, these particles also following pitch angle dependent paths (Oberhagemann & Mann, 2020a, 2020b). The key issue being that the overall ion anisotropy in the pressure-carrying parts of the proton energy distribution needs to be sufficient to destabilize the ballooning mode due to a transition toward a more overall parallel pressure anisotropic state.

During the growth phase, the perpendicular particle energy decreases as the magnetic field decreases, conserving the first adiabatic invariant. As the tail stretches, the field line length increases, and the average parallel velocity decreases as the second adiabatic invariant is conserved. We hypothesize and expect the rate of decrease of the

perpendicular energy to be higher than that of the parallel energy, such that betatron deceleration is faster than the Fermi deceleration, resulting in an increase in parallel temperature anisotropy during the growth phase. Moreover, the proton fluxes at low pitch angles could remain nearly constant during tail stretching, as is observed in Figures 4c–4f. As we show in the superposed epoch statistics, the increase in the ratio of 30°/90° flux and the decrease in the pressure anisotropy factor toward onset, is a strong indication that the flux distribution is parallel anisotropic at substorm onset. The observed increase in parallel anisotropy with energy, as demonstrated in Figures 4g–4j, and panels g–j in Figures S5, S6, and S7 in Supporting Information S1, suggests that the protons become more anisotropic with increasing energy in the energy range of MAGPD. The observed peak pressure anisotropy of ~ -0.12 at GOES 15 corresponds to a symmetric pressure anisotropy factor of ~ -0.14, calculated using Equation 1 from Oberhagemann and Mann (2020b). Considering an average plasma beta of ∼4 (Pu et al., 1992) at geosynchronous altitudes during the substorm late growth phase, along with an example pressure gradient of $\alpha = 5$, the symmetric pressure anisotropy factor falls outside the stable parameter space (refer to Figure 3 in Oberhagemann and Mann (2020b)), indicating the possible transition to a ballooning unstable state. Almost 75% of the substorm events where the satellite is to the west of the onset see an anisotropy factor of −0.1 and below. The signatures are more enhanced in GOES 15 than GOES 13, presumably because the former is closer to the magnetic equator. Note that the orbit of the GOES 13 and 15 satellites means that they sweep through different magnetic field lines in the nightside magnetosphere, and observe the particle distributions along the world-line of the satellites at fixed geosynchronous altitudes.

Overall, the observations and analysis we present here show signatures of the development of increasing energetic proton parallel pressure anisotropy during the substorm growth phase, immediately before the onset. This is supportive of Oberhagemann and Mann (2020b) theory, where they proposed that the development of increasingly parallel pressure anisotropy is destabilizing and could trigger a ballooning instability. The ballooning instability would then lead to the onset of the expansion phase. It is of course possible that the stretching of the tail in the late growth phase provides a more parallel temperature anisotropic energetic proton population in the near-Earth plasmasheet which plays no causative role in triggering substorm onset. Indeed, Sorathia et al. (2020), using small-scale global simulations of the late growth phase magnetotail, have shown how a small-scale local minima in Bz may be formed and associated with ballooning and the generation of auroral beads. However, these authors point out that this may or may not be associated with the subsequent triggering of substorm onset in the near-Earth plasmasheet. Regardless, a number of papers have highlighted the potential connection between the triggering of ballooning modes and the subsequent onset of magnetic reconnection in the mid-tail (e.g., Zhu et al., 2017, and references therein). Certainly, the observations presented here indicate energetic proton parallel pressure anisotropy at substorm onset at geosynchronous orbit, consistent with the Oberhagemann and Mann (2020b) anisotropic pressure ballooning substorm onset model. Future research to investigate if this relationship is causal is warranted.

Data Availability Statement

The OMNI data can be obtained through Papitashvili and King (2020). The isolated substorm list (Ohtani & Gjerloev, 2020) is available from the SuperMAG collaboration website (SuperMAG, 2023). GOES 13 and GOES 15 satellite data can be accessed at NOAA NCEI (2023). The Tsyganenko T89 magnetic field model (Tsyganenko, 1989) was analyzed using the python geopack library (Tian, 2023).

Acknowledgments
This work was supported by an NSERC Discovery Grant to IRM, the NSERC CREATE grant for the International Space Mission (ISM) training program, and the Canadian Space Agency. IJR is funded in part by STFC Grant ST/X001008/1, and NERC Grants NE/V002554/2 and NE/W003198/1. AWS was supported by NERC Independent Research Fellowship NE/W009129/1. We acknowledge the substorm timing list identified by the Ohtani and Gjerloev technique (Ohtani & Gjerloev, 2020), the SMU and SML indices (Newell & Gjerloev, 2011); and the SuperMAG collaboration (Gjerloev, 2012).

References

Akasofu, S. I. (1964). The development of the auroral substorm. *Planetary and Space Science*, *12*(4), 273–282. https://doi.org/10.1016/0032-0633(64)90151-5

Akasofu, S.-I. (1965). Dynamic morphology of auroras. *Space Science Reviews*, *4*(4), 498–540. https://doi.org/10.1007/BF00177092

Akasofu, S.-I. (1977). Auroras and auroral particles. In S.-I. Akasofu (Ed.), *Physics of magnetospheric substorms* (pp. 71–136). Springer Netherlands. https://doi.org/10.1007/978-94-010-1164-8_3

Akasofu, S.-I. (2017). Auroral substorms: Search for processes causing the expansion phase in terms of the electric current approach. *Space Science Reviews*, *212*(1), 341–381. https://doi.org/10.1007/s11214-017-0363-7

Angelopoulos, V., McFadden, J. P., Larson, D., Carlson, C. W., Mende, S. B., Frey, H., et al. (2008). Tail reconnection triggering substorm onset. *Science*, *321*(5891), 931–935. https://doi.org/10.1126/science.1160495

Baker, D. N., Higbie, P. R., Hones, E. W., & Belian, R. D. (1978). High-resolution energetic particle measurements at 6.6 R_e, 3. Low-energy electron anisotropies and short-term substorm predictions. *Journal of Geophysical Research*, *83*(A10), 4863–4868. https://doi.org/10.1029/JA083iA10p04863

Baker, D. N., Pulkkinen, T. I., Angelopoulos, V., Baumjohann, W., & McPherron, R. L. (1996). Neutral line model of substorms: Past results and present view. *Journal of Geophysical Research*, *101*(A6), 12975–13010. https://doi.org/10.1029/95JA03753

Birn, J., Thomsen, M. F., Borovsky, J. E., Reeves, G. D., McComas, D. J., & Belian, R. D. (1997). Characteristic plasma properties during dispersionless substorm injections at geosynchronous orbit. *Journal of Geophysical Research*, *102*(A2), 2309–2324. https://doi.org/10.1029/96JA02870

Chen, M. W., Roeder, J. L., Fennell, J. F., Lyons, L. R., & Schulz, M. (1998). Simulations of ring current proton pitch angle distributions. *Journal of Geophysical Research*, *103*(A1), 165–178. https://doi.org/10.1029/97JA02633

Chen, Y., Friedel, R. H. W., Henderson, M. G., Claudepierre, S. G., Morley, S. K., & Spence, H. E. (2014). REPAD: An empirical model of pitch angle distributions for energetic electrons in the Earth's outer radiation belt. *Journal of Geophysical Research: Space Physics*, *119*(3), 1693–1708. https://doi.org/10.1002/2013JA019431

De Michelis, P., Daglis, I. A., & Consolini, G. (1997). Average terrestrial ring current derived from AMPTE/CCE-CHEM measurements. *Journal of Geophysical Research*, *102*(A7), 14103–14111. https://doi.org/10.1029/96JA03743

De Michelis, P., Daglis, I. A., & Consolini, G. (1999). An average image of proton plasma pressure and of current systems in the equatorial plane derived from AMPTE/CCE-CHEM measurements. *Journal of Geophysical Research*, *104*(A12), 28615–28624. https://doi.org/10.1029/1999JA900310

Denton, M. H., Thomsen, M. F., Korth, H., Lynch, S., Zhang, J. C., & Liemohn, M. W. (2005). Bulk plasma properties at geosynchronous orbit. *Journal of Geophysical Research*, *110*(A7), A07223. https://doi.org/10.1029/2004JA010861

Freeman, M. P., & Morley, S. K. (2009). No evidence for externally triggered substorms based on superposed epoch analysis of IMF B_z. *Geophysical Research Letters*, *36*(21), L21101. https://doi.org/10.1029/2009GL040621

Fu, H., Yue, C., Zong, Q., Zhou, X., Yu, Y., Li, Y., et al. (2023). Substorm influences on plasma pressure and current densities inside the geosynchronous orbit. *Journal of Geophysical Research: Space Physics*, *128*(3), e2022JA031099. https://doi.org/10.1029/2022JA031099

Gjerloev, J. W. (2012). The SuperMAG data processing technique. *Journal of Geophysical Research*, *117*(A9), A09213. https://doi.org/10.1029/2012JA017683

Henderson, M. G. (2021). Key elements of auroral substorm development and their relationship to recent observations of detached sub-auroral phenomena including STEVE-like emissions. *Journal of Atmospheric and Solar-Terrestrial Physics*, *218*, 105600. https://doi.org/10.1016/j.jastp.2021.105600

Jaynes, A. N., Lessard, M. R., Rodriguez, J. V., Donovan, E., Loto'aniu, T. M., & Rychert, K. (2013). Pulsating auroral electron flux modulations in the equatorial magnetosphere. *Journal of Geophysical Research: Space Physics*, *118*(8), 4884–4894. https://doi.org/10.1002/jgra.50434

Kalmoni, N. M. E., Rae, I. J., Murphy, K. R., Forsyth, C., Watt, C. E. J., & Owen, C. J. (2017). Statistical azimuthal structuring of the substorm onset arc: Implications for the onset mechanism. *Geophysical Research Letters*, *44*(5), 2078–2087. https://doi.org/10.1002/2016GL071826

Kalmoni, N. M. E., Rae, I. J., Watt, C. E. J., Murphy, K. R., Samara, M., Michell, R. G., et al. (2018). A diagnosis of the plasma waves responsible for the explosive energy release of substorm onset. *Nature Communications*, *9*(1), 4806. https://doi.org/10.1038/s41467-018-07086-0

King, J. H., & Papitashvili, N. E. (2005). Solar wind spatial scales in and comparisons of hourly Wind and ACE plasma and magnetic field data. *Journal of Geophysical Research*, *110*(A2), 2004JA010649. https://doi.org/10.1029/2004JA010649

Loto'aniu, P. T. M., Califf, S., Redmon, R. J., & Singer, H. J. (2020). Chapter 21—Magnetic field observations from the GOES-R series. In S. J. Goodman, T. J. Schmit, J. Daniels, & R. J. Redmon (Eds.), *The GOES-R series* (pp. 251–259). Elsevier. https://doi.org/10.1016/B978-0-12-814327-8.00021-4

Lui, A. T. Y. (1991). A synthesis of magnetospheric substorm models. *Journal of Geophysical Research*, *96*(A2), 1849–1856. https://doi.org/10.1029/90JA02430

Lui, A. T. Y. (2003). Cause of magnetospheric substorms. *Plasma Physics and Controlled Fusion*, *45*(6), 841–852. https://doi.org/10.1088/0741-3335/45/6/301

Lui, A. T. Y. (2004). Potential plasma instabilities for substorm expansion onsets. *Space Science Reviews*, *113*(1), 127–206. https://doi.org/10.1023/B:SPAC.0000042942.00362.4e

Lui, A. T. Y., Angelopoulos, V., LeContel, O., Frey, H., Donovan, E., Sibeck, D. G., et al. (2008). Determination of the substorm initiation region from a major conjunction interval of THEMIS satellites. *Journal of Geophysical Research*, *113*(A1), A00C04. https://doi.org/10.1029/2008JA013424

Lui, A. T. Y., Chang, C.-L., Mankofsky, A., Wong, H.-K., & Winske, D. (1991). A cross-field current instability for substorm expansions. *Journal of Geophysical Research*, *96*(A7), 11389–11401. https://doi.org/10.1029/91JA00892

Mann, I. R., Milling, D. K., Rae, I. J., Ozeke, L. G., Kale, A., Kale, Z. C., et al. (2008). The upgraded CARISMA magnetometer array in the THEMIS era. *Space Science Reviews*, *141*(1), 413–451. https://doi.org/10.1007/s11214-008-9457-6

McPherron, R. L. (1979). Magnetospheric substorms. *Reviews of Geophysics*, *17*(4), 657–681. https://doi.org/10.1029/RG017i004p00657

McPherron, R. L., Russell, C. T., & Aubry, M. P. (1973). Satellite studies of magnetospheric substorms on August 15, 1968: 9. Phenomenological model for substorms. *Journal of Geophysical Research*, *78*(16), 3131–3149. https://doi.org/10.1029/JA078i016p03131

Morley, S. K., & Freeman, M. P. (2007). On the association between northward turnings of the interplanetary magnetic field and substorm onsets. *Geophysical Research Letters*, *34*(8), L08104. https://doi.org/10.1029/2006GL028891

Newell, P. T., & Gjerloev, J. W. (2011). Evaluation of SuperMAG auroral electrojet indices as indicators of substorms and auroral power. *Journal of Geophysical Research*, *116*(A12), 2011JA016779. https://doi.org/10.1029/2011JA016779

NOAA NCEI. (2023). GOES online data repository [Dataset]. https://www.ngdc.noaa.gov/stp/satellite/goes/dataaccess.html

Oberhagemann, L. R., & Mann, I. R. (2020a). Increasingly parallel pressure anisotropic ballooning: Substorm growth phase drift orbits resulting in a locally ballooning unstable geomagnetic tail. *Journal of Geophysical Research: Space Physics*, *125*(10), e2020JA028022. https://doi.org/10.1029/2020JA028022

Oberhagemann, L. R., & Mann, I. R. (2020b). A new substorm onset mechanism: Increasingly parallel pressure anisotropic ballooning. *Geophysical Research Letters*, *47*(2), e2019GL085271. https://doi.org/10.1029/2019GL085271

Ohtani, S. (2001). Substorm trigger processes in the magnetotail: Recent observations and outstanding issues. *Space Science Reviews*, *95*(1), 347–359. https://doi.org/10.1023/A:1005231122496

Ohtani, S., & Gjerloev, J. W. (2020). Is the substorm current wedge an ensemble of wedgelets?: Revisit to midlatitude positive bays. *Journal of Geophysical Research: Space Physics*, *125*(9), e2020JA027902. https://doi.org/10.1029/2020JA027902

Papitashvili, N. E., & King, J. H. (2020). OMNI 1-min data [Dataset]. *NASA Space Physics Data Facility*. https://doi.org/10.48322/45BB-8792

Pu, Z. Y., Korth, A., & Kremser, G. (1992). Plasma and magnetic field parameters at substorm onsets derived from GEOS 2 observations. *Journal of Geophysical Research*, *97*(A12), 19341–19349. https://doi.org/10.1029/92JA01732

Rae, I. J., Mann, I. R., Angelopoulos, V., Murphy, K. R., Milling, D. K., Kale, A., et al. (2009). Near-Earth initiation of a terrestrial substorm. *Journal of Geophysical Research*, *114*(A7), A07220. https://doi.org/10.1029/2008JA013771

Rae, I. J., Watt, C. E. J., Mann, I. R., Murphy, K. R., Samson, J. C., Kabin, K., & Angelopoulos, V. (2010). Optical characterization of the growth and spatial structure of a substorm onset arc. *Journal of Geophysical Research*, *115*(A10), A10222. https://doi.org/10.1029/2010JA015376

Rodriguez, J. V. (2014). Goes 13-15 mage/pd pitch angles algorithm theoretical basis document version 1.0, 28. Retrieved from https://ngdc.noaa.gov/stp/satellite/goes/doc/MAGEPD_PitchAngles_Processing_ATBD_v1.0.pdf

Rowland, W., & Weigel, R. S. (2012). Intracalibration of particle detectors on a three-axis stabilized geostationary platform. *Space Weather*, *10*(11), S11002. https://doi.org/10.1029/2012SW000816

Sergeev, V. A., Angelopoulos, V., & Nakamura, R. (2012). Recent advances in understanding substorm dynamics. *Geophysical Research Letters*, *39*(5), L05101. https://doi.org/10.1029/2012GL050859

Sibeck, D. G., McEntire, R. W., Lui, A. T. Y., Lopez, R. E., & Krimigis, S. M. (1987). Magnetic field drift shell splitting: Cause of unusual dayside particle pitch angle distributions during storms and substorms. *Journal of Geophysical Research*, *92*(A12), 13485–13497. https://doi.org/10.1029/JA092iA12p13485

Smith, A. W., Rae, I. J., Forsyth, C., Watt, C. E. J., Murphy, K. R., & Mann, I. R. (2020). Diagnosing the time-dependent nature of magnetosphere-ionosphere coupling via ULF waves at substorm onset. *Journal of Geophysical Research: Space Physics*, *125*(11), e2020JA028573. https://doi.org/10.1029/2020JA028573

Sorathia, K. A., Merkin, V. G., Panov, E. V., Zhang, B., Lyon, J. G., Garretson, J., et al. (2020). Ballooning-interchange instability in the near-Earth plasma sheet and auroral beads: Global magnetospheric modeling at the limit of the MHD approximation. *Geophysical Research Letters*, *47*(14), e2020GL088227. https://doi.org/10.1029/2020GL088227

SuperMAG. (2023). SuperMAG substorm event list [Dataset]. https://supermag.jhuapl.edu/substorms/

Tian, S. (2023). The geopack and Tsyganenko models in Python. [Software]. https://pypi.org/project/geopack/

Tsyganenko, N. A. (1989). A magnetospheric magnetic field model with a warped tail current sheet. *Planetary and Space Science*, *37*(1), 5–20. https://doi.org/10.1016/0032-0633(89)90066-4

Zhu, P., Bhattacharjee, A., Sangari, A., Wang, Z., & Bonofiglo, P. (2017). Three-dimensional geometry of magnetic reconnection induced by ballooning instability in a generalized Harris sheet. *Physics of Plasmas*, *24*(2), 024503. https://doi.org/10.1063/1.4976994